Effects of a Fillet on the Flow Past a Wing-Body Junction

W. J. Devenport,* N. K. Agarwal,† M. B. Dewitz,‡ R. L. Simpson,§ and K. Poddar¶
Virginia Polytechnic Institute and State University, Blacksburg, Virginia 24061

Measurements are presented to demonstrate the effects of a simple fillet on the flow of a turbulent boundary layer past an idealized wing-body junction. The time-averaged flow structure in the vicinity of the wing and in the wake of the wing-body junction is considered, as well as the unsteadiness of the horseshoe vortex. The effects of angle of attack and approach boundary-layer thickness are also examined.

Introduction

THE flow of a turbulent boundary layer on a surface past a wing or other protuberance from that surface occurs in many practical situations of engineering interest. In general, wing-body junction flows are complex and poorly understood. Most research in this area has been done on cylindrical wings mounted to flat surfaces (e.g., Fig. 1). In this situation, the turbulent boundary layer is strongly influenced by the pressure field generated by the wing. Spanwise pressure gradients skew the boundary layer as it encounters the wing, turning some of the initially spanwise boundary-layer vorticity in the streamwise direction. Adverse streamwise pressure gradients ahead of the wing leading edge cause flow separation here and the formation of a separation line on the surface that trails around the wing. The existence of this separation allows the skew-induced streamwise vorticity close to the wing to become concentrated into a clearly identifiable structure (at least in the time average). This structure is commonly called a horseshoe vortex since it is wrapped around the nose of the wing. Its legs trail downstream in the corner between the wing wake and the boundary layer.

The horseshoe vortex has a number of characteristics that, in most practical situations, are undesirable. The horseshoe vortex is subject to large-scale, low-frequency bistable unsteadiness that appears to be generated in the nose region.[1-3] In some applications, such as the junction between a submarine hull and sail, this almost certainly leads to the generation of unwanted noise. The vortex acts to bring high-momentum, freestream fluid into the corner between the wing and surrounding surface. This energizes the flow here and it also greatly increases the surface shear stresses[4] adding to the drag and, when thermal effects are important, increasing the heat transfer.[5,6] The trailing legs of the vortex persist very far downstream of the wing. They increase the nonuniformity of the wake and can interfere with the operation of other devices downstream (such as propulsor blades).

There is, thus, some incentive to find simple modifications to the wing-body junction geometry that alter the characteristics of the horseshoe vortex or eliminate it as an organized structure. Perhaps the simplest modification is to change the wing shape. Mehta[7] has shown that the circulation within the streamwise legs of the vortex and the apparent size of those legs decreases with the radius of the wing nose. Rood and Anthony[8] have shown that the shape of the tail of the wing also has an effect. Their measurements, carried out on a wing at slight angle of attack, show that a tail that produces a greater adverse pressure gradient increases the size of the vortex legs and the area over which their unsteadiness is felt.

The influence of large fairings in the corner between the nose of the wing and the surface (of the type shown in Fig. 2a) has been examined by Sung et al.[9] and Kubendran et al.[10] Kubendran et al.'s flow visualizations, performed with a laminar approach boundary layer, suggest that this type of flow-control device eliminates the leading-edge separation. Not surprisingly, Sung et al. found that it also attenuated the strength of the vortex legs downstream, decreasing the nonuniformity of the wake. Pierce et al.[11] investigated the effect of a steep triangular fairing with a sharp leading edge (Fig. 2b). Although this device greatly attenuated the vortex, its sharp leading edge did not make it suitable for situations in which the wing was at angle of attack. Some purely computational work on the effects of leading- and trailing-edge fairings has been done by Sung and Lin.[12]

The modification of a fillet around the entire base of the wing (Fig. 3b) has been used for many years on aircraft because in some situations it can substantially reduce the interference drag of the junction.[13] Pierce et al.[11] recently studied the effects of three such fillets. However, because of the largely qualitative nature of their measurements, they were unable to come to any clear conclusions concerning the relative merits of these devices. Scheiman and Kubendran[14] studied the effects of a fillet on one side of an asymmetric wing with a sharp leading edge. Although they made no direct comparisons with an unfilleted case, they concluded that the fillet improved the flow characteristics near the wing trailing edge by eliminating regions of low-momentum fluid.

The purpose of this paper is to present measurements to demonstrate clearly some effects of adding a simple fillet to an idealized wing-body junction. The unsteadiness generated in the nose region and the time-averaged structure of the flow around the wing and in the wing wake are considered. The effects of angle of attack and approach boundary-layer thickness are also examined.

Apparatus and Measurement Techniques

A detailed account of the apparatus and measurement techniques is given by Dewitz.[15] They are only briefly described here.

Wing Models

The two wing models used are shown in Figs. 3a and 3b. The baseline wing (Fig. 3a) is cylindrical. Its cross section consists of a 3:2 elliptical nose, with its major axis aligned with the

Presented as Paper 89-0986 at the AIAA 2nd Shear Flow Control Conference, Tempe, AZ, March 13-16, 1989; received July 21, 1989; revision received Dec. 21, 1989.

*Assistant Professor, Department of Aerospace and Ocean Engineering. Senior Member AIAA.
†Research Associate, Department of Aerospace and Ocean Engineering. Senior Member AIAA.
‡Graduate Assistant, Department of Aerospace and Ocean Engineering.
§Jack E. Cowling Professor, Department of Aerospace and Ocean Engineering. Associate Fellow AIAA.
¶Research Associate, Department of Aerospace and Ocean Engineering.

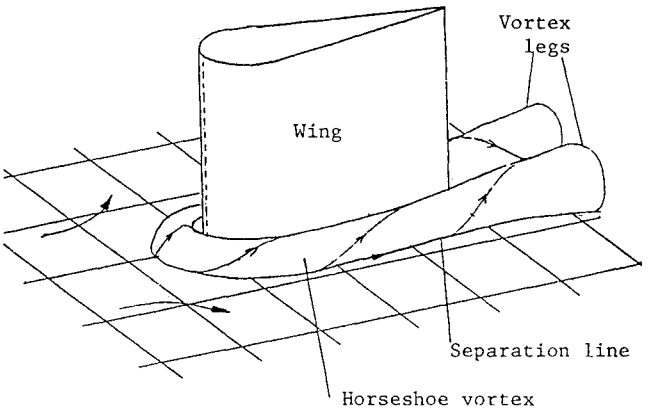

Fig. 1 Flow around a cylindrical wing mounted normal to a surface.

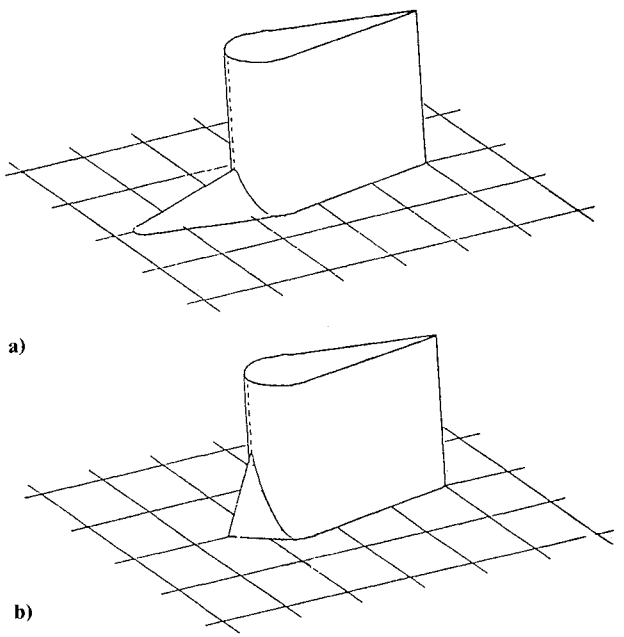

Fig. 2 Leading-edge fairlings: a) as studied by Sung et al.[9] and Kubendran et al.[10]; b) as studied by Pierce et al.[11]

chord, and a NACA 0020 tail. It has a maximum thickness T of 7.17 cm, a chord of 30.5 cm, and a span of 22.9 cm. The wing with fillet (Fig. 3b) is identical to the baseline wing except for the addition of a simple fillet wrapped around its base. The cross section of the fillet, in any plane normal to the wing surface and surrounding wall, is a quarter circle with a radius of 3.81 cm (0.53T) centered 3.81 cm from both the wall and wing. The fillet thus provides a smooth transition from the wing surface to the surrounding wall.

Both models were constructed from aluminum using a numerically controlled milling machine. In practice, a feather edge, like that required by the fillet, cannot be machined with any accuracy. The fillet was therefore cut off between 3.2 and 3.0 cm from the wing surface, leaving a step between 0.5 and 0.8 mm in height. During measurements, this step was covered using wax so that the surface of the fillet was continuous with the surrounding test wall.

For measurements at zero angle of attack, a boundary-layer transition trip was attached to both sides of the baseline wing. This consisted of a 6.4-mm-wide strip of 120-grade sandpaper attached with its leading edge 28.2 mm downstream of the leading edge of the wing. Surface oil-flow visualizations performed with and without the trip showed it to have no significant effect on the flow outside the wing boundary layer. No trips were used with the fillet.

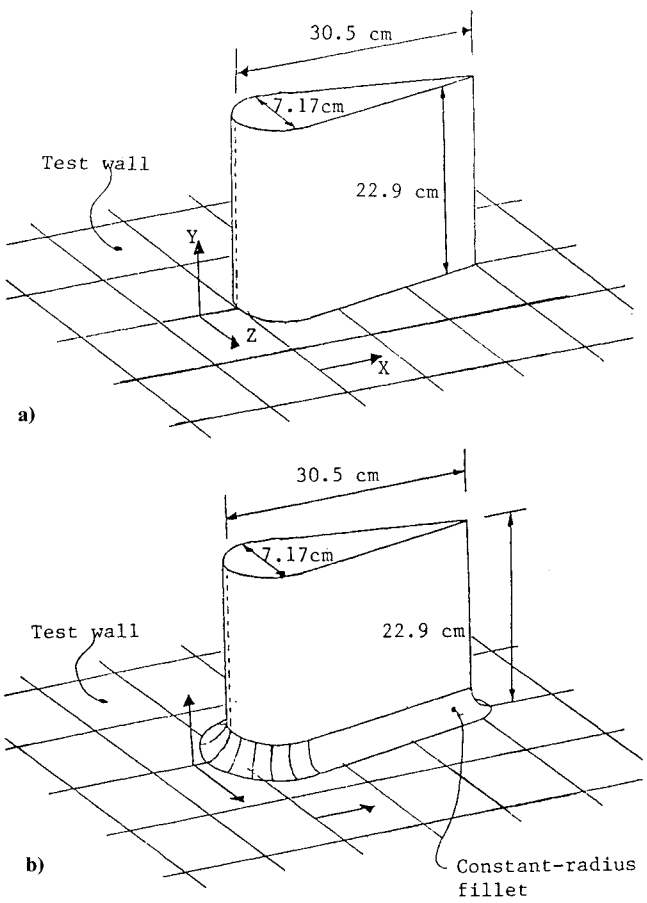

Fig. 3 Wing models: a) baseline wing; b) wing with fillet.

Wind Tunnels

The wing, both with and without fillet, was tested with two different approach boundary layers. Measurements with the wing at zero angle of attack were made in a small boundary-layer tunnel. The test section of this tunnel was 8-m long and 0.91-m wide and had a rectangular cross section. In the absence of the wing, there was a zero-pressure-gradient flow through the test section. This consisted of a uniform low-turbulence (<0.2%) mainstream and, depending on the configuration of the wind tunnel, either a thick or thin equilibrium turbulent boundary layer on the flat, 0.91-m-wide test wall. The height of the test section was different for the two boundary layers and increased slightly with distance downstream. Where the wing was mounted the height was 26.7 and 22.9 cm with the thick and thin boundary layers, respectively. There was thus, a gap of 3.8 cm between the upper wall of the wind tunnel and the top of the wing when the thick boundary layer was present. With the wing in place, inserts for the wind tunnel side walls were used to minimize blockage-induced pressure gradients. The nominal approach mainstream velocity U_{ref} was 27 m/s for the thick boundary layer and 32 m/s for the thin. The boundary-layer thickness, measured with the baseline wing mounted in the wind tunnel, 2.15 wing thicknesses T upstream of its leading edge, were 0.50T and 0.25T. These correspond to momentum thickness Reynolds numbers of 6.6 and 4.5 $\times$ 10^3, respectively.

Measurements at 0-, 6-, and 12-deg angle of attack were made in the Virginia Tech Stability Wind Tunnel. This large, general-purpose wind tunnel had a test section 7.3-m long with a square cross section 1.8 m on edge. Flow through the empty test section was uniform and had a very low turbulence intensity (<0.05%). The test wall used in this wind tunnel consisted of a large flat plate spanning the test section at its mid height. The wing was mounted at the center span of the plate and pivoted to angle of attack about a point one-third of the way

from the leading to the trailing edge. For measurements in this wind tunnel, a cap was attached to the otherwise blunt top of the wing to avoid the complex flow that would be produced. The shape of the cap was that of half a body of revolution generated by rotating the cross section of the baseline wing about its chord line. All measurements in the stability tunnel were carried out at a freestream velocity of 32 m/s. At this speed, the flat plate produced a boundary layer with nominally the same properties as the thin boundary layer of the small wind tunnel.

Measurement Techniques

To give a general view of the flows produced both with and without the fillet, surface oil-flow visualizations and mean surface pressure measurements were made on the wing surfaces and surrounding test walls. Oil-flow visualizations were performed using a mixture of kerosene, titanium dioxide, and oleic acid according to the procedure described by Maltby.[16] Visualizations were preserved using the method of Sutton,[17] described by Devenport and Simpson.[18] Mean surface static pressures were measured through more than 300 static pressure ports using a Scanivalve system and two Setra model 239 pressure transducers. The Scanivalve system was controlled, and pressures were read through a Data Translation DT2801-A converter by an IBM AT computer.

Detailed hot-wire velocity measurements were made in the wakes of the unmodified wing and the wing with fillet using two rakes of hot-wire probes custom built by Dantec. Each rake consisted of 16 sensors arranged at different heights along a probe stem mounted normal to the test wall. Up to 10 of the wires were operated at any one time using constant-temperature anemometers of the type designed by Miller[19] and modified by Simpson et al.[20] Unlinearized outputs from these anemometers were recorded by the IBM AT using the DT2801-A converter. Signals were linearized in the computer and the mean and root mean square (rms) values calculated. The rakes were calibrated in the wind tunnels against a pitot-static tube using a least-squares fit to King's law. Temperature variations with time in the stability tunnel were substantial (typically 2 to 3°C/h). The rakes were therefore calibrated frequently and corrections for temperature drift, determined using the method of Bearman,[21] were applied.

Measurements of turbulent surface pressure fluctuations were made at the same streamwise location as the velocity measurements. Knowles Electronics model BT 1753 condenser microphones, mounted flush with the test wall, were used. These have a pinhole orifice of 0.51 mm in diameter. Microphones respond to acoustic noise and vibration as well as turbulent pressure fluctuations. To eliminate these unwanted contributions, the cancellation technique of Agarwal and Simpson,[22] employing two closely spaced microphones (11 mm apart in this case), was used. This method, which exploits the fact that acoustic and vibration signals remain correlated over much longer time delays than do turbulent pressure signals, is demonstrated in Fig. 4. Here, a pressure spectrum, measured in the two-dimensional zero-pressure-gradient boundary layer produced in the stability wind tunnel with the wing model removed, is shown before applying the technique and after. Plotted in terms of the inner variables $\phi(\omega)/\rho^2 U_\tau^2 \nu$ and $\omega\nu/U_\tau^2$ [where $\phi(\omega)$ is the power spectral density, ω the angular frequency, and U_τ the friction velocity], the processed spectrum agrees fairly well with the results of McGrath and Simpson[23] for an equilibrium boundary layer of similar momentum-thickness Reynolds number. It also shows the $f^{-0.7}$, f^{-1}, and f^{-5} variations normally expected in this type of flow.[24]

Part of the two-component laser Doppler velocimeter (LDV) described by Simpson and Chew[25] was used to measure histograms of the streamwise component of velocity in the regions of leading-edge separation generated by the wing with fillet. Extensive work by Devenport and Simpson[1-3] has shown that velocity histograms measured here with the baseline wing tend to have two peaks (i.e., they are bimodal). These histograms are produced by low-frequency bistable velocity fluctuations that result from large-scale unsteadiness in the size, position, and structure of the horseshoe vortex. The LDV measurements were, therefore, expected to show the effects of the fillet on the presence of this unsteadiness.

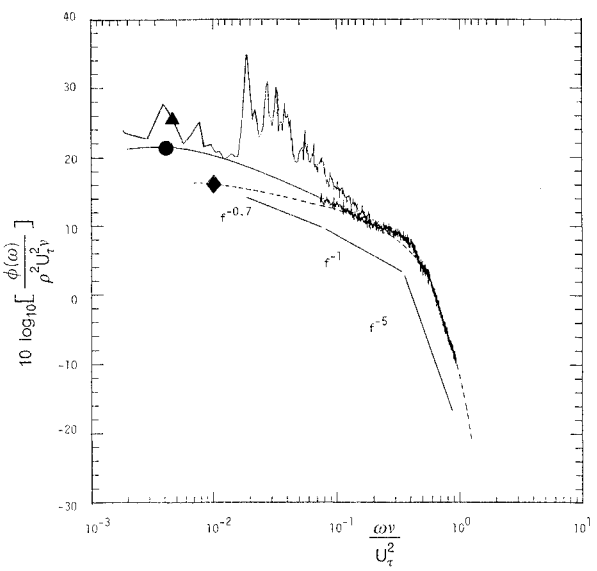

Fig. 4 Power spectrum of surface pressure fluctuations measured in the stability tunnel with the wing model removed ($Re_\theta = 7.59 \times 10^3$): ▲ raw spectrum; ● spectrum processed using technique of Agarwal and Simpson[22]; ◆ data of McGrath and Simpson[23] ($Re_\theta = 8.196 \times 10^3$).

Results and Discussion

Results will be presented using the coordinate system (X, Y, Z) defined in Fig. 3. The coordinate system is fixed in the wind tunnel, with the spanwise and streamwise coordinates X and Z originating from a line coincident with the leading edge of the wing when the wing is at zero angle of attack. The coordinate Y is measured normal to the test wall. Distances will be normalized using the maximum thickness of the wing T (7.17 cm) or the wing chord (30 cm).

Table 1 Summary of measurements made with the baseline wing and wing with fillet

Boundary layer: (δ/T)	Thick (.5)	Thin (.26)	Thin (.26)	Thin (.26)
Reynolds number Re_θ:	6.6×10^3	4.5×10^3	4.5×10^3	4.5×10^3
Angle of attack of wing:	0 deg	0 deg	6 deg	12 deg
Oil-flow visualizations on test wall and wings	✓	✓	✓	✓
Mean surface pressures on test wall and wings		✓	✓	✓
Hot-wire surveys of wake at $X/C = 3$	✓	✓	✓	
LDV measurements near nose at at $Z/T = 0$	✓	✓		
Microphone measurements in wake at $X/C = 3$	✓	✓	✓	✓

Table 2 Uncertainty intervals calculated using the method of Kline and McClintock[26]

Quantity	Uncertainty
Mean pressure coefficient C_p	$\pm 0.006 C_p$
Turbulence normal stress $\overline{u^2}/U_e^2$	±6.0%
Y location of hot wire	$\pm 0.006T$
Z location of hot wire	$\pm 0.05T$
Pressure spectrum level	±1.5 dB
Total rms pressure coefficient C_p'	±8.0%

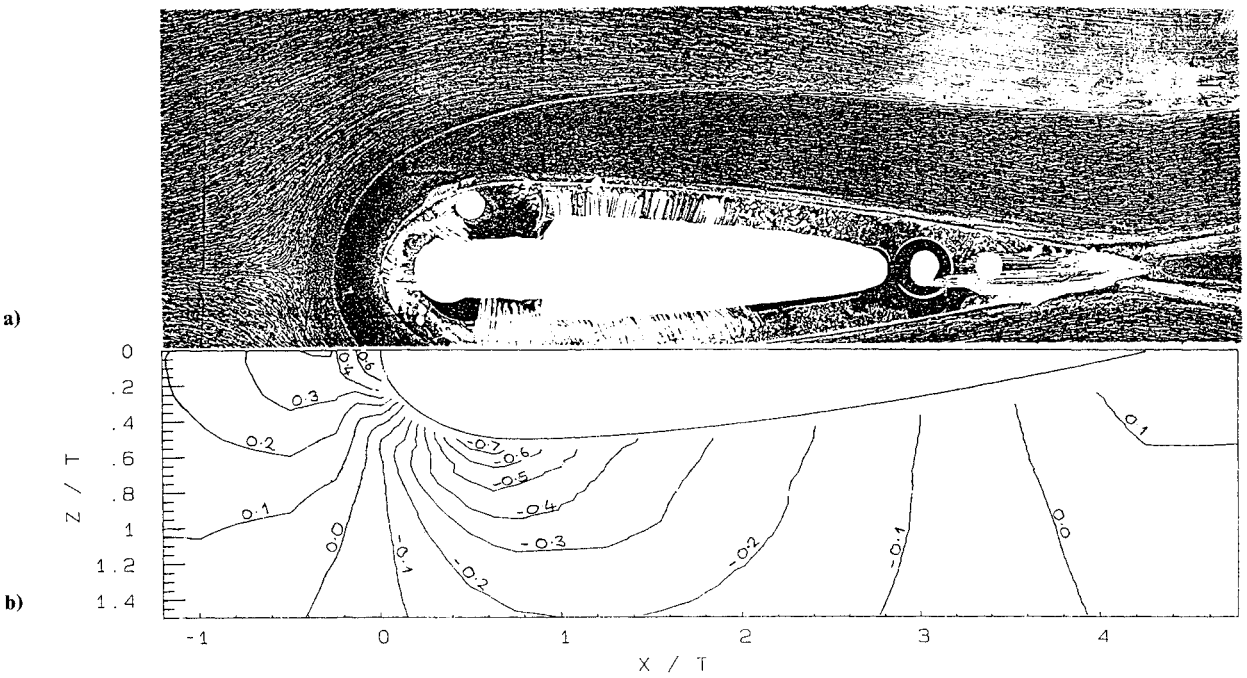

Fig. 5 Flow on the test wall in the vicinity of the baseline wing at zero angle of attack with the thin boundary layer: a) surface oil-flow visualization; b) contours of mean surface pressure coefficient C_p.

The measurements made are summarized in Table 1. Because of the volume of results, only a representative sample will be presented here. Uncertainties in measurements, calculated using the method of Kline and McClintock,[26] are listed in Table 2.

Surface Oil-Flow Visualizations

A surface oil-flow visualization performed on the test wall surrounding the baseline wing, at zero angle of attack in the thin boundary layer, is shown in Fig. 5a. Since the visualization is symmetrical, only half of it is shown here. A line of separation, wrapped around the wing, originates at a saddle (or separation) point in the plane of symmetry $0.45T$ upstream of the wing leading edge. (Strictly speaking, a line of attachment, coincident with the plane of symmetry, also passes through this saddle point.) This so-called leading-edge separation occurs because of the strong adverse pressure gradient imposed by the wing in this region. Surprisingly, away from the saddle point, the separation line is not initially marked by much accumulation of titanium dioxide. Instead, pigment has built up on a line formed closer to the wing that crosses the plane of symmetry $0.27T$ upstream of the wing. Close to the plane of symmetry, this line is not a separation or reattachment since the oil streaks here clearly pass through it. Measurements made by Devenport and Simpson[4] show this to be a line of low streamwise shear. This line divides the separated flow into two distinct regions: a strip of high-surface shear stresses adjacent to the wing, generated by the time-averaged action of the horseshoe vortex, and a crescent-shaped region of apparently lower shear stress upstream (see Devenport and Simpson[2,4] for other results confirming these observations). The line of low shear merges with the leading-edge separation line just downstream of the wing maximum thickness. From this point on, the separation line diverges slowly from the wing surface; the spanwise distance between the two is $0.86T$ at the trailing edge. Just upstream of the trailing edge separation occurs in the corner between the wing and wall creating a fishtail-like pattern in the wake.

Figure 6a is the corresponding oil-flow visualization performed with the fillet. Unlike in Fig. 5a, the edge of the blank region in Fig. 6a corresponds to the edge of the fillet and not the vertical surface of the wing. The fillet does not prevent leading-edge separation, and, qualitatively, the flow appears much the same as around the baseline wing. With the fillet, the saddle point and the origin of the line of low shear occur farther upstream at $X/T = -0.69$ and -0.49, respectively, and the spanwise distance from the wing surface to the leading-edge separation line at the trailing edge is increased to $1.15T$. In general, the fillet appears to displace the flow structure away from the wing surface in a manner that suggests that it increases the effective radius of the nose. We might therefore expect, in light of Mehta's[7] results, for the fillet to increase the size and strength of the horseshoe vortex.

Changing the boundary-layer thickness or placing the wing models at angle of attack produced no significant qualitative changes in the surface oil-flow visualizations. Quantitative changes, expressed in terms of the distances L_{sep}, L_{lols}, W_s, and W_p are summarized in Table 3. The L_{sep} and L_{lols} are, respectively, the distances from the saddle point and the line of low shear to the vertical part of the wings measured along the incoming attachment line. The W is the distance, measured normal to the wing chord, from the trailing edge of the wing to the primary separation line either on the suction (subscript s) or pressure (subscript p) sides. The W_s and W_p are obviously equal for the zero angle-of-attack cases.

The factor of two difference in thickness between the boundary layers has remarkably little effect on the oil-flow visualizations of the baseline wing and wing with fillet. In both cases, there is only a small increase on the distance of the saddle point from the wing leading edge, whereas the other parameters remain almost constant. This suggests that much of the structure of this type of wing-body junction flow may be almost independent of boundary-layer thickness δ/T and Reynolds number Re_θ. This is consistent with the observations of Baker[27] on the flow past a circular cylinder mounted normal to a flat plate. Placing the wing models at angle of attack produced moderate or small increases in L_{sep} and L_{lols} for both cases. As is indicated by the values of W_s and W_p, the oil-flow visualizations retained a surprising degree of symmetry downstream of the nose region at angle of attack.

Mean Surface Pressure Measurements

Contours of mean surface pressure coefficient C_p, constructed from measurements made on the test wall surrounding the baseline wing at zero angle of attack in the thin boundary layer, are shown in Fig. 5b. Measurements made on the

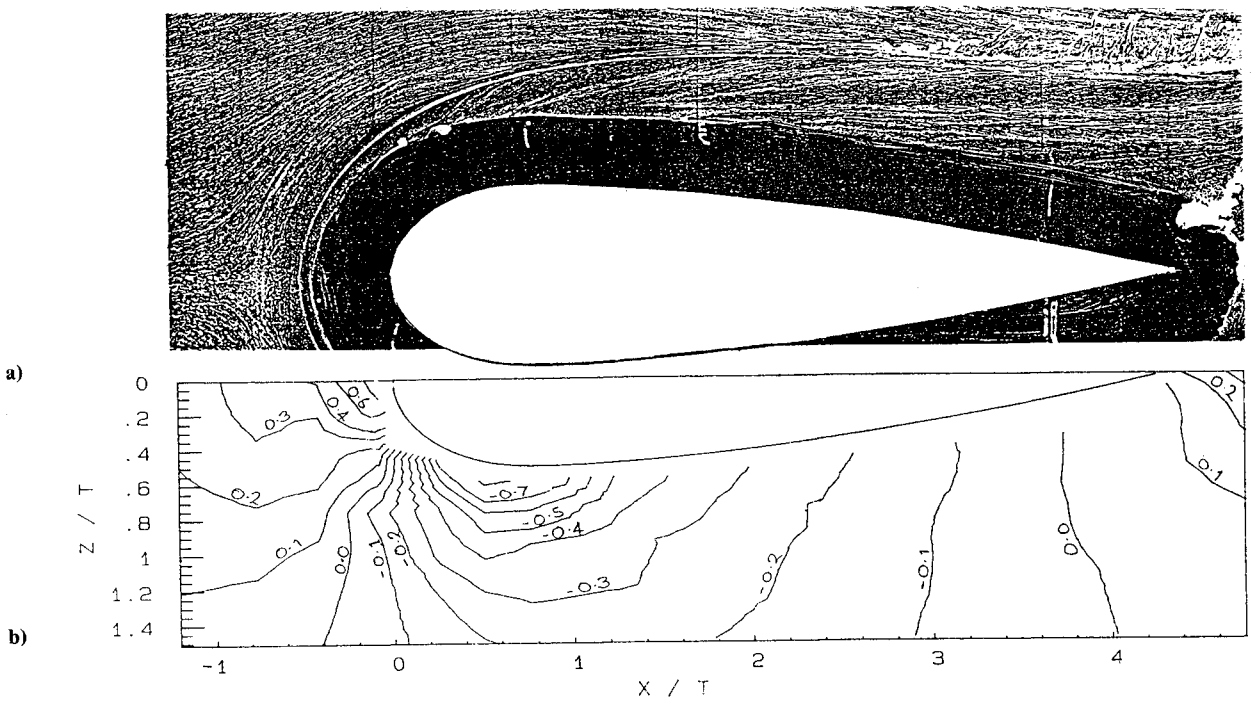

Fig. 6 Flow on the test wall in the vicinity of the wing with fillet at zero angle of attack with the thin boundary layer: a) surface oil-flow visualization; b) contours of mean surface pressure coefficient C_p.

test wall and fillet surface under identical conditions with the fillet are represented in Fig. 6b. The C_p, defined as $(p - p_{ref})/(p_0 - p_{ref})$ where p_0 and p_{ref} are the stagnation and static pressures of the undisturbed mainstream, has an uncertainty of about 0.006.

Both pressure distributions show the same qualitative features: a strong adverse pressure gradient upstream of the wing leading edge (that causes separation here), a strong favorable pressure gradient between the leading edge and maximum-thickness location (as the flow accelerates around the nose), and a region of pressure recovery that extends from near the maximum-thickness location to the trailing edge. In general, values of C_p measured with the fillet (Fig. 6b) are greater in magnitude than those measured at corresponding points with the unmodified wing. This is at least partly because the surface of the fillet, on which pressures close to the wing were measured, rises up through the test-wall boundary layer. However, this difference is also seen on the test wall surrounding the fillet. (Note for example where the contour $C_p = -0.2$ intersects the X axis in Figs. 5b and 6b.) The favorable pressure gradient experienced by the near-wall flow as it negotiates the wing nose and the pressure recovery it experiences over the downstream part of the wing are therefore greater in the presence of the fillet. An interesting feature of the surface-pressure maps is the shallow "valley" in the pressure that occurs in front of the nose of both wing models. With the baseline wing, this feature, visible as a distortion of the pressure contours, is centered on a line approximately $0.3T$ from the wing surface. With the fillet, this valley is less pronounced and occurs further from the vertical surface of the wing. The valley is most likely due to a lowering of the pressure in the vicinity of the core of the horseshoe vortex, suggesting that the vortex is formed further from the wing in the presence of the fillet. This is consistent with the surface oil-flow visualizations.

As with the visualizations, the surface pressure distributions for the two cases retain the same qualitative features at angle of attack.

Table 3 Summary of surface oil-flow visualizations on the test walls

Wing	Boundary layer	Angle of attack, deg	L_{sep} / T	L_{lols} / T	W_s / T	W_p / T
Baseline						
	Thick	0	0.47	0.28	0.86	0.86
	Thin	0	0.45	0.27	0.86	0.86
	Thin	6	0.47	0.27	0.96	0.94
	Thin	12	0.54	0.31	1.11	0.95
With Fillet						
	Thick	0	0.72	0.49	1.17	1.17
	Thin	0	0.69	0.49	1.15	1.15
	Thin	6	0.71	0.50	1.24	1.14
	Thin	12	0.74	0.51	1.30	1.17

Hot-Wire Velocity Measurements in the Wake Region

Detailed measurements of the streamwise components of mean velocity $\bar{U}$ and turbulence normal stress $\overline{u'^2}$ were made in a spanwise plane at $X/C = 3$ ($X/T = 12.7$) to give a cross-sectional view of the wake of the wing-body junction. Figures 7a–7f show contours of $\overline{u'^2}$ drawn from these measurements. (Mean-velocity contours will not be presented here since they show much the same qualitative effects and trends.) The $\overline{u'^2}$ is normalized on the velocity of the mainstream at $X/C = 3$ (U_e) and has an uncertainty of about $\pm 6\%$. With the wing at zero angle of attack, measurements were only made on one side of the plane of symmetry. The complete cross sections of the flow shown in Figs. 7a–7d were therefore obtained by reflecting these data about $Z = 0$.

Figure 7a shows measurements made downstream of the baseline wing at zero angle of attack in the thin boundary layer. The contours clearly show the extent of the test-wall boundary layer and the wing wake. The streamwise legs of the horseshoe vortex may be seen through the distortion they cause to the otherwise horizontal contours of the test-wall boundary layer. Between $Z/T = 0.3$ and 0.7, where the legs tend to bring low-turbulence mainstream fluid toward the wall, the contours of $\overline{u'^2}/U_e^2$ are depressed. Between $Z/T = 0.7$ and 2, turbulence levels and the boundary-layer thickness are elevated by the presence of the vortex. The primary cause of the increase in $\overline{u'^2}$ is probably the additional mixing of boundary-layer fluid that must accompany the rotational motion of the vortex. Another possible source, since the vortex legs are associated with spanwise gradients of velocity, is a spanwise meandering of these legs. Such a mechanism

might also account for the flattened appearance of the region occupied by the legs in the time-averaged view of Fig. 7a. The fact that $\overline{u'^2}/U_e^2$ reaches a maximum at $Z/T = 1.4$ in a region where mean-velocity measurements show the vortex to be lifting fluid away from the wall suggests yet another mechanism. It may be that this lifting action, which creates a region of low-momentum fluid adjacent to the wall, destabilizes the boundary layer here, much as an adverse streamwise pressure gradient would.

The effect of adding the fillet may be seen by comparing Figs. 7a and 7b. The fillet increases the cross-sectional area of the region affected by the legs of the horseshoe vortex as well as the distortion of the $\overline{u'^2}/U_e^2$ contours. The maximum boundary-layer thickness in the vicinity of the vortex legs, defined by the maximum height of the $0.0001U_e^2$ contour, is $0.92T$, 25% greater than without the fillet. There would seem to be two possible causes of these effects. The fillet may magnify the size and strength of the vortex legs (as would be expected if it increases the effective radius of the wing nose) or it may increase the extent of their unsteady motions in the spanwise plane. Since the magnitudes of $\overline{u'^2}/U_e^2$ near the center of the vortex legs are very similar with and without the fillet, the first cause seems more likely. This conclusion is supported by the fact that the legs of the vortex appear further apart with the fillet, the maximum in $\overline{u'^2}/U_e^2$ occurring at $Z/T = 1.59$ in this case. Stronger vortex legs would move apart more rapidly under the action of their images in the test wall.

With the thick approach boundary layer (Figs. 7c and 7d), the qualitative effects of the fillet are the same. This is because the structure of the wing wake and vortex legs is only slightly affected by the differences between the thick and thin approach boundary layers. A comparison of Figs. 7a with 7c and 7b with 7d shows differences in the shapes and positions of the $\overline{u'^2}/U_e^2$ contours, which, in the regions dominated by the wing wake and vortex legs, are small when compared to the factor of two change in approach boundary-layer thickness. With the fillet, the maximum in boundary-layer thickness in the vicinity of the vortex is only 5% higher in the thick boundary layer. This figure is 15% for the unmodified wing. For both configurations, the peak in $\overline{u'^2}/U_e^2$ produced by the vortex occurs about 10% closer to the plane of symmetry with the thick boundary layer. Turbulence levels are on average slightly lower in the vortex legs with the thick boundary layer. This may be because the vortex legs are embedded deeper in the thick boundary layer and, therefore, on average mix fluid with less difference in streamwise velocity.

The fact that the structure of the horseshoe vortex appears only weakly dependent on the approach boundary-layer thickness is consistent with our surface oil-flow visualizations and mean surface pressure measurements.

The effects of placing the wing at 6-deg angle of attack may be seen by comparing Figs. 7a with 7e and 7b with 7f. At this angle, the trailing edge of the wing is located at $Z/T = 0.3$. The most obvious effect of angle of attack is to deflect the wing wake and horseshoe vortex in the positive Z direction (toward the pressure side of the wing). For both models, the legs are deflected less than the wing wake, the suction-side leg ending up closer to the wing wake, and the pressure-side leg

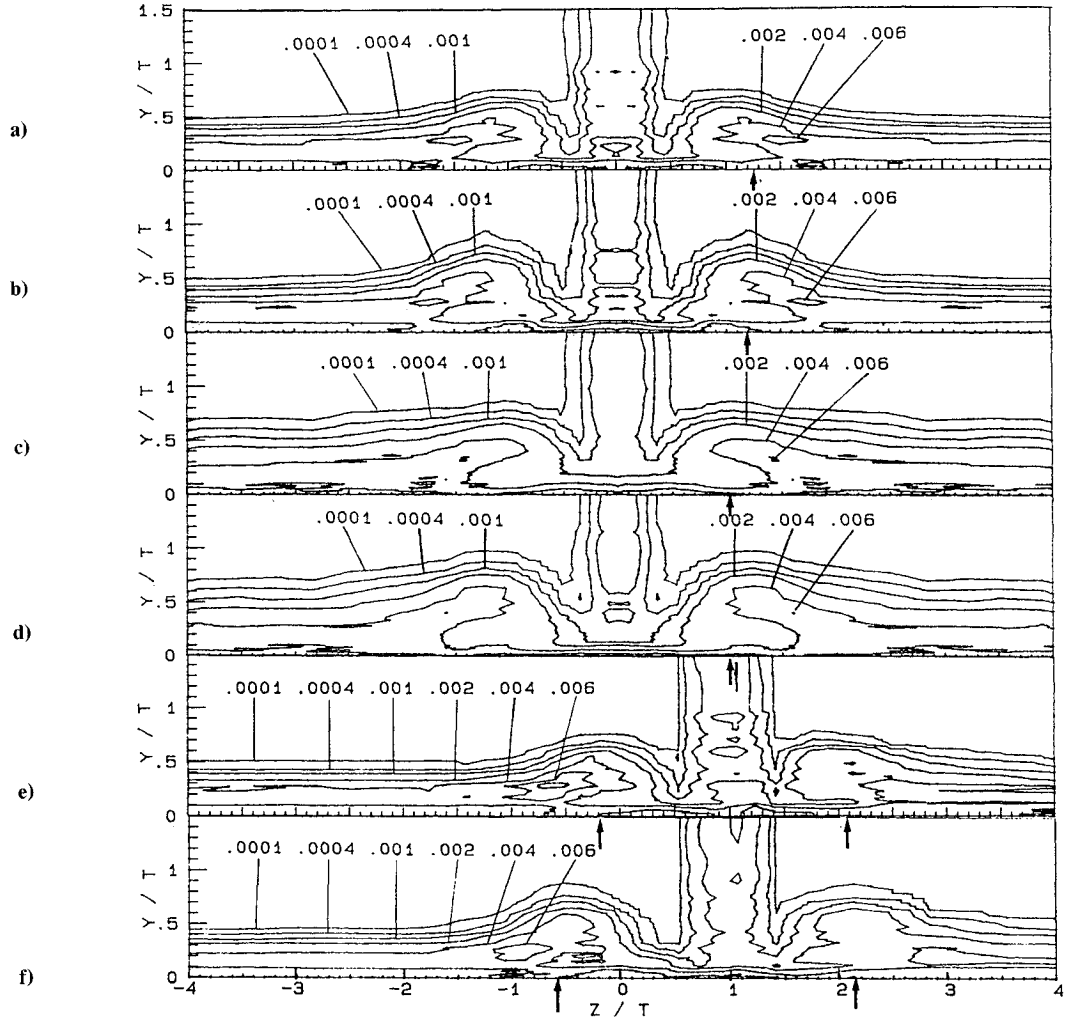

Fig. 7 Contours of $\overline{u'^2}/U_e^2$ in a spanwise plane at $X/C = 3$ (arrows show locations of microphone measurements); a) baseline wing, thin boundary layer (BL), 0-deg angle of attack (AOA); b) with fillet, thin BL, 0-deg AOA; c) baseline wing, thick BL, 0-deg AOA; d) with fillet, thick BL, 0-deg AOA; e) baseline wing, thin BL, 6-deg AOA; and f) with fillet, thin BL, 6-deg AOA.

Table 4 Total pressure fluctuation levels at $X/C = 3$ expressed in terms of C_p'

Angle of attack, Deg / Location	Boundary layer	Baseline wing	Wing with fillet
0	Thick		
0	Thin	0.0095	0.0100
6 / Suction side	Thin	0.0108	0.0097
6 / Pressure side	Thin	0.0083	0.0158
12 / Suction side	Thin	0.0109	0.0111
12 / Pressure side	Thin	0.0113	0.0133

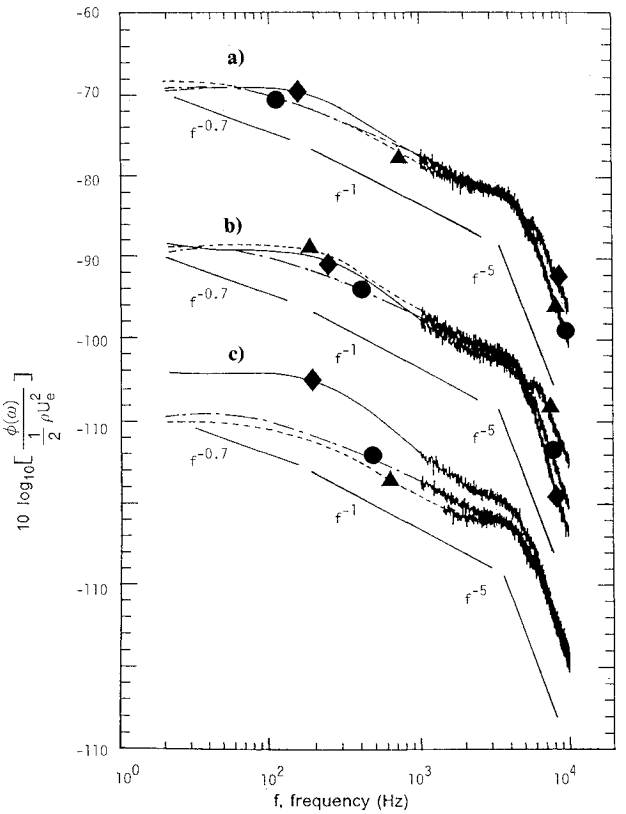

Fig. 8 Surface pressure spectra measured at $X/C = 3$ with the thin boundary layer, ▲ baseline wing; ◆ fillet; ● no wing model: a) 0-deg angle of attack; b) 6-deg (suction side); and c) 6-deg (pressure side).

ending up further from the wing wake than at zero angle of attack. In both cases, turbulence levels are lower in the suction-side leg and higher in the pressure-side leg than at zero angle of attack. Most of the qualitative effects of adding the fillet are the same as at zero angle of attack; the apparent size and separation of the vortex legs and their distortion of the boundary-layer edge all increase.

Microphone Measurements in the Wake Region

Microphone measurements were made at $X/C = 3$ under the legs of the horseshoe vortex (exact locations are indicated by the arrows in Fig. 7). Overall pressure-fluctuation levels are listed in Table 4 in terms of the coefficient $C_p' = \sqrt{p'^2}/\frac{1}{2}\rho U_e^2$ (uncertainty ±8%). Selected pressure spectra, measured with the thin approach boundary layer, are plotted in Fig. 8 in terms of $\phi(\omega)/\frac{1}{2}\rho U_e^2$ and dimensional frequency. For comparison, this figure also includes the two-dimensional boundary-layer spectrum of Fig. 4.

In all cases, except on the suction side of the wing at 6-deg angle of attack, the fillet increases the level of surface-pressure fluctuations. This increase is fairly uniform across the spectrum (Figs. 8a–8c), suggesting that the fillet enhances turbulent activity over a broad range of scales. The actual shape of the spectrum is in all cases fairly similar to that of the two-dimensional boundary layer. All spectra display f^{-1} and f^{-5} regions.

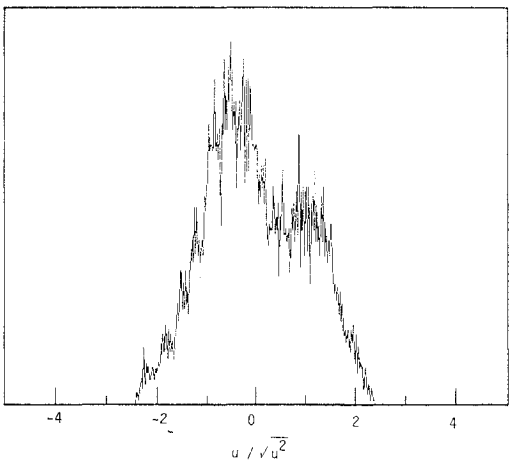

Fig. 9 Bimodal histogram of velocity fluctuations measured at $X/T = -0.62$, $Y/T = 0.02$, $Z/T = 0$; wing with fillet, 0-deg angle of attack, thin boundary layer.

LDV Measurements Near the Nose

The single-component LDV was used to search the regions of leading-edge separation generated by the wing with fillet for bimodal histograms of streamwise velocity fluctuations. Histograms of this type characterize the large-scale unsteadiness present with the baseline wing.[1-3] Measurements were made in the plane of symmetry at zero angle of attack with both thick and thin approach boundary layers. For both boundary layers, clearly bimodal histograms (of the type shown in Fig. 9) were observed in regions just in front of the upstream edge of the fillet. The fillet, therefore, did not eliminate the bimodal unsteadiness.

Conclusions

Measurements have been presented to demonstrate the effects of a simple fillet on the flow of a turbulent boundary layer past an idealized wing-body junction. The fillet was of uniform radius, equal to 0.53 wing thickness, and was wrapped around the entire base of the wing. Measurements, made with two approach boundary layers of different thickness and with the wing at 0-, 6- and 12-deg angle of attack, suggest the following conclusions.

1) The fillet does not prevent leading-edge separation or, apparently, the formation of a horseshoe vortex. Instead, it displaces the separated-flow structure away from the wing surface in a manner that suggests it increases the effective radius of the nose of the wing.

2) The fillet does not eliminate the large-scale bistable unsteadiness that characterizes flow in the nose region of the unmodified wing.

3) The fillet increases the spectral level of surface pressure fluctuations under the streamwise legs of the horseshoe vortex.

4) The fillet increases the distortion of the time-averaged boundary layer structure produced by the streamwise legs of the horseshoe vortex and the area over which it occurs. This could indicate that the fillet increases the size and strength of the vortex.

5) Placing the wing at angle of attack or changing the approach boundary-layer thickness does not appear to alter the qualitative effects of the fillet on the structure of the horseshoe vortex.

With the possible exception of its effect on the interference drag (which could not be discerned from the measurements made in this investigation), the fillet does not modify the flow past the wing-body junction in a desirable way. In applications where elimination or attenuation of the horseshoe vortex or its

unsteady motions are required, this type of device clearly should not be used. A flow-control device that eliminates leading-edge separation is likely to be more effective.

Acknowledgments

This work was supported by the Office of Naval Research under Contract N00014-88-C-0291.

References

[1]Devenport, W. J., and Simpson, R. L., "Turbulence Structure Near the Nose of a Wing-Body Junction," AIAA Paper 87-1310, 1987.

[2]Devenport, W. J., and Simpson, R. L., "LDV Measurements in the Flow Past a Wing-Body Junction," Fourth International Symposium on Applications of Laser Anemometry to Fluid Mechanics, Lisbon, Portugal, 1988.

[3]Devenport, W. J., and Simpson, R. L., "Time-Dependent and Time-Averaged Turbulence Structure Near the Nose of a Wing-Body Junction," *Journal of Fluid Mechanics,* Vol. 210, 1990, pp. 23–55.

[4]Devenport, W. J., and Simpson, R. L., "Time Dependent Structure in Wing-Body Junction Flows," *Turbulent Shear Flows VI,* Springer-Verlag, 1989, pp. 232–248.

[5]Graziani, R. A., Blair, M. F., Taylor, J. R., and Mayle, R. E., "An Experimental Study of End Wall and Aerofoil Surface Heat Transfer in a Large Scale Turbine Blade Cascade," American Society of Mechanical Engineers, Paper 79-GT-99, 1979.

[6]Blair, M. F., "Heat-Transfer in the Vicinity of a Large-Scale Obstruction in a Turbulent Boundary Layer," *Journal of Propulsion and Power,* Vol. 1, 1985, pp. 158–160.

[7]Mehta, R. D., "Effect of Wing-Nose Shape on the Flow in a Wing-Body Junction," *Aeronautical Journal,* Vol. 77, 1984, pp. 456–460.

[8]Rood, E. P., and Anthony, D. G., "Tail Profile Effects on Unsteady Large Scale Flow Structure in the Wing and Plate Junction," *Forum on Unsteady Flow,* edited by P. H. Rothe, American Society of Mechanical Engineers, ASME FGD 27, 1985.

[9]Sung, C.-H., Yang, C.-I., and Kubendran, L. R., "Control of Horseshoe Vortex Juncture Flow Using Fillet," Symposium on Hydrodynamic Performance Enhancement for Marine Applications, Newport, RI, Oct. 1988.

[10]Kubendran, L. R., Bar-Sever, A., and Harvey, W. D., "Flow Control in a Wing/Fuselage Type Juncture," AIAA Paper 88-0614, Jan. 1988.

[11]Pierce, F. J., Frangistas, G. A., and Nelson, D. J., "Geometry-Modification Effects on a Junction-Vortex Flow," *Proceedings of the Symposium on Hydrodynamic Performance Enhancement for Marine Applications,* Oct. 1988, pp. 37–44.

[12]Sung, C.-H., and Lin, C.-W., "Numerical Investigation on the Effect of Fairing on the Vortex Flows Around Airfoil/Flat-Plate Junctures," *Proceedings of the AIAA 26th Aerospace Sciences Meeting,* AIAA, Washington, DC, Jan. 1988.

[13]Hoerner, S. F., *Fluid Dynamic Drag,* Hoerner, 1965.

[14]Scheiman, J., and Kubendran, L. R., "Juncture Flow Measurements Using Laser Velocimetry," AIAA Paper 85-1612, July 1985.

[15]Dewitz, M., "The Effect of a Fillet on a Wing/Body Junction Flow," M.S. Thesis, Virginia Polytechnic Institute and State Univ., Blacksburg, VA, 1988.

[16]Maltby, R. L., "Flow Visualization in Wind Tunnels Using Indicators," AGARD AG 70, 1962.

[17]Sutton, E. P., private communication, 1985.

[18]Devenport, W. J., and Simpson, R. L., "Some Time-Dependent Features of Turbulent Appendage-Body Juncture Flows," *Proceedings of the 16th Symposium on Naval Hydrodynamics,* National Academy of Sciences, Washington, DC, 1989, p. 461.

[19]Miller, J. A., "A Simple Linearized Hot-Wire Anemometer," *Journal of Fluids Engineering,* Vol. 98, 1976, pp. 550–557.

[20]Simpson, R. L., Heizer, K. W., and Nasburg, R. E., "Performance Characteristics of a Simple Linearized Hot-Wire Anemometer," *Journal of Fluids Engineering,* Vol. 101, 1979, pp. 381–382.

[21]Bearman, P. W., "Corrections for the Effect of Ambient Temperature Drift on Hot-Wire Measurement in Incompressible Flow," DISA Info., Vol. 11, 1971, pp. 25–30.

[22]Agarwal, N. K., and Simpson, R. L., "A New Technique for Obtaining the Turbulent Pressure Spectrum from the Surface Pressure Spectrum," *Journal of Sound and Vibration* (to be published).

[23]McGrath, B. E., and Simpson, R. L., "Some Features of Surface Pressure Fluctuations in Turbulent Boundary Layers with Zero and Favorable Pressure Gradients," NASA CR-4051, 1987.

[24]Blake, W. K., *Mechanics of Flow Induced Sound and Vibration,* Vol. 2, Academic, Orlando, FL, 1986, pp. 534–540.

[25]Simpson, R. L., and Chew, Y.-T., "Measurements in Steady and Unsteady Separated Turbulent Boundary Layers," *Laser Velocimetry and Particle Sizing,* edited by H. D. Thompson and W. H. Stevenson, Hemisphere, 1979, pp. 179–196.

[26]Kline, S. J., and McClintock, F. A., "Describing Uncertainties in Single-Sample Experiments," *Mechanical Engineering,* Vol. 75, 1953, pp. 3–8.

[27]Baker, C. J., "The Turbulent Horseshoe Vortex," *Journal of Engineering and Industrial Aerodynamics,* Vol. 6, 1980, pp. 9–23.